In vivo pulse-echo measurement of apparent broadband attenuation and Q factor in cortical bone: a preliminary study

Jean-Gabriel Minonzio, Chao Han, Didier Cassereau, Quentin Grimal

In vivo pulse-echo measurement of apparent broadband attenuation and Q factor in cortical bone: A preliminary study

Jean-Gabriel Minonzio[a,b,c,*], Chao Han[a], Didier Cassereau[a], Quentin Grimal[a]

[a] *Sorbonne Université, INSERM UMR S 1146, CNRS UMR 7371, Laboratoire d'Imagerie Biomédicale, 75006 Paris, France*
[b] *Escuela de Ingeniería Informática, Universidad de Valparaíso, Valparaíso, Chile*
[c] *Centro de Investigación y Desarrollo en Ingeniería en Salud, Universidad de Valparaíso, Valparaíso, Chile.*

Abstract

Quantitative UltraSound (QUS) methods have been introduced to assess cortical bone health at the radius and tibia through the assessment of Cortical Thickness (Ct.Th), Cortical Porosity (Ct.Po) and bulk wave velocities. Ultrasonic attenuation is another QUS parameter which is not currently used. We assess the feasibility of *in vivo* measurement of ultrasonic attenuation in cortical bone with a broadband transducer with 3.5 MHz-center frequency. Echoes from the periosteal and endosteal interfaces were fitted with Gaussian pulses using sparse signal processing. Then, the slope of the Broadband Ultrasonic Attenuation (Ct.nBUA) in cortical bone and quality factor Q_{11}^{-1} were calculated with a parametric approach based on the center-frequency shift. Five human subjects were measured at the one-third distal radius with pulse-echo ultrasound, and reference data was obtained with high-resolution X-ray peripheral computed tomography (Ct.Th and Cortical volumetric Bone Mineral Density, Ct.vBMD). Ct.Th was used in the calculation of Ct.nBUA while Q_{11}^{-1} is obtained solely from ultrasound data. The values of Ct.nBUA

*Corresponding Author: Jean-Gabriel Minonzio; Escuela de Ingeniería en Informática, Universidad de Valparaíso, General Cruz 222, 2362905 Valparaíso, Email: jean-gabriel.minonzio@uv.cl

(6.7±2.2 dB.MHz.$^{-1}$.cm^{-1}) and Q_{11}^{-1} (8.6±3.1 %) were consistent with the literature data and were correlated to Ct.vBMD ($R^2 = 0.92$, $p < 0.01$, $RMSE = 0.56$ dB.MHz^{-1}.cm^{-1}, and $R^2 = 0.93$, $p < 0.01$, RMSE= 0.76%). This preliminary study suggests that the attenuation of an ultrasound signal propagating in cortical bone can be measured *in vivo* at the one-third distal radius and that it provides an information on bone quality as attenuation values. It remains to ascertain that Ct.nBUA and Q_{11}^{-1} measured here exactly reflect the true (intrinsic) ultrasonic attenuation in cortical bone. Measurement of attenuation may be considered useful for assessing bone health combined with the measurement of cortical thickness, porosity and bulk wave velocities in multimodal cortical bone QUS methods.

Keywords: cortical bone, broadband ultrasonic attenuation, Quantitative Ultrasound, *in vivo* measurement, Orthogonal Matching Pursuit, sparse reconstruction, Q factor

---

Introduction

Osteoporosis fracture risk is currently assessed using Dual energy X-ray Absorptiometry (DXA) in order to assess areal Bone Mineral Density (aBMD). However, DXA has strong limitations, in particular it lacks sensitivity (Briot et al., 2013; Siris, 2004) and is not appropriate to monitor cortical bone (Choksi et al., 2018). Cortical bone, the dense tissue that forms the outer shells of the bones, represents about 80% of the human skeleton mass and plays an important role in the skeletal mechanical stability (Holzer et al., 2009; Zebaze et al., 2010; Bala et al., 2014). Aging and bone pathologies are associated with cortical thinning (Nishiyama et al., 2010) and weakening of the bone material mechanical quality reflected in an increase of Cortical Porosity (Ct.Po) (Kral et al., 2017) or a decrease of Cortical volumetric Bone Mineral Density (Ct.vBMD (CT.vBMD) (Ostertag et al., 2016; Paranhos Neto et al., 2019).

Several quantitative ultrasound (QUS) approaches have been introduced to assess cortical bone health at the radius and tibia. Some aim at assessing Cortical Thickness (Ct.Th) assuming a nominal value of ultrasound velocity using pulse-echo (Karjalainen et al., 2008), axial transmission (Moilanen, 2008), or through transmission measurements (Sai et al., 2010). Other approaches are designed for a combined estimation of Ct.Th and Ct.Po or bulk wave velocities using axial transmission measurements of several guided wave modes (Foiret et al., 2014; Minonzio et al., 2019) or adaptative pulse-echo imaging with a transducer array (Renaud et al., 2018, 2020). Ultrasonic attenuation is another QUS parameter which has been exploited for several decades in soft tissues (Mamou and Oelze, 2013) and trabecular bone (Langton and Njeh, 2008); however, until now, it has received little consideration in cortical bone QUS.

Ex vivo studies on cuboid specimens have established that ultrasonic attenuation of bulk waves in cortical bone is related to mass density (Bernard et al., 2015) and to Ct.vBMD (Sasso et al., 2008). Also, simulations have suggested that the scattering of ultrasound by the cavities of the pore network is one important mechanism of attenuation (Yousefian et al., 2018, 2021; Iori et al., 2020). It follows that, in addition to ultrasonic velocities measured with QUS approaches (Grimal and Laugier, 2019), attenuation could be indicative of the mechanical quality of cortical bone as it is related to Ct.Po and Ct.vBMD.

There has been a few attempts to measure attenuation in *ex vivo* bone

specimens. Zheng et al. (2007) measured in pulse echo mode a bovine femur specimen and estimated the slope of the frequency-dependent attenuation coefficient (also refered to as "spectral ratio method") to estimate the so-called Cortical normalized Broadband Ultrasonic Attenuation (Ct.nBUA). They later used a parametric approach introduced by Kuc et al. (1976) which related attenuation to the shift of the center frequency (also refered to as "peak frequency method") (Zheng et al., 2009). Dencks et al. (2008) also used this parametric approach and measured nBUA in proximal femurs in through-transmission. However, these values of nBUA can hardly be interpreted in terms of bulk cortical bone material properties because ultrasound propagated along a complex path through both cortical and trabecular bone. As far as we know, *in vivo* measurements of attenuation in cortical bone have not yet been reported.

The aim of this paper was to assess the feasibility of *in vivo* measurement of attenuation in cortical bone. We have conducted a preliminary study on the radius of five human subjects. Ultrasound echoes stemming from the normal-incidence reflection on the outer (periosteal) and inner (endosteal) cortical bone interfaces were recorded and processed with Orthogonal Matching Pursuit (OMP) to retrieve the time delay, the temporal echo width and the frequency shift of the center frequency from which Ct.nBUA and the quality factor Q were calculated with a parametric approach (Kuc et al., 1976). The quality factor is introduced as a quantity related to the dissipation of energy which can be measured without the need of the knowledge of the bulk wave velocity. Ultrasound parameters Ct.nBUA and Q were compared to reference values of Ct.vBMD of each subject which were obtained with High-Resolution X-ray peripheral Quantitative Computed Tomography (HR-pQCT). The results are of interest for the development of future multimodal cortical bone QUS approaches estimating bone structural (thickness) and material (porosity, velocities, attenuation) properties for the evaluation of bone health.

1. Method

1.1. Extraction of echoes

The signal received in the pulse-echo ultrasound measurement is modeled as a sum of two Gaussian pulses $s_i(t)$, or Gabor functions, i.e., the product of a Gaussian function with a complex sinusoid (Demirli and Saniie, 2001)

$$y(t) = \sum_{i=1}^{2} s_i(t) + n(t) = \sum_{i=1}^{2} A_i \exp[-\frac{(t-t_i)^2}{2\sigma_{t_i}^2}] \cos[2\pi f_i(t-t_i)] + n(t), \quad (1)$$

where σ_{t_i} is the standard deviation of the temporal Gaussian function, f_i is the central frequency, t_i is the group delay and A_i is the amplitude of i-th echo. The error between the model and the measured signal, including noise, is $n(t)$. The first and second echoes correspond to the reflections on the outer (periosteal) and inner (endosteal) bone surfaces, respectively.

For further use, we write the temporal Fourier transform of one echo as

$$S_i(f) = \frac{A_i}{\sqrt{2\pi}\sigma_{fi}} \exp[-\frac{(f-f_i)^2}{2\sigma_{fi}^2}] \exp[-j2\pi f t_i], \quad (2)$$

where the standard deviation of the Gaussian function σ_{f_i} satisfies $2\pi\sigma_{f_i} = 1/\sigma_{t_i}$. The -6dB frequency bandwidth, or full width at half maximum, is related to σ_{f_i}, and is equal to $2\sqrt{2\ln(2)}\sigma_{f_i} \approx 2.35\sigma_{f_i}$.

The echoes are isolated using a sparse signal processing method in the time domain which provides the quantities σ_{t_i}, f_i, t_i, and A_i $(i = 1, 2)$. The method is detailed in Appendix ; shortly, the signal model, given by (1), discretized in time can be represented as

$$\mathbf{y} = \mathbf{D}\mathbf{x} + \mathbf{n}, \quad (3)$$

where $\mathbf{y}$ and $\mathbf{n}$ are $N_t \times 1$ vectors corresponding to the sampling of $y(t)$ and $n(t)$ at N_t discrete time points, respectively. Likewise, $\mathbf{x}$ is a $N_m \times 1$ vector collecting the N_m relative amplitudes of the echoes. In a sparse point of view, only a few elements of this vector are non zero. Finally, $\mathbf{D}$ is a $N_t \times N_m$ matrix corresponding the so-called dictionary. Each column $\mathbf{d}(t; \sigma_{t_m}, f_m, t_m)$, with $m = 1 \cdots M$, of $\mathbf{D}$ is one of the M Gabor functions discretized at N_t time points, defined by the set of parameters (σ_{t_m}, f_m, t_m). For a given measurement $y(t)$, the problem amounts to determine the two non-zero components of $\mathbf{x}$, which indices yield the set of parameters corresponding to the two echoes. This is done by sparse reconstruction with Orthogonal Matching Pursuit (OMP) (Tropp and Gilbert, 2007). The details of the construction of the dictionary and of the implementation of OMP can be found in Appendix.

1.2. Measurement of attenuation: Theory

The cortical bone layer is modeled locally as a plate of thickness Ct.Th. We assume that the temporal signals can be decomposed into monochromatic plane waves propagating in bone at normal incidence on the plate surfaces. The complex wavenumber is denoted $(k + i\alpha)$, where α is the imaginary part and is assumed to present a linear attenuation with frequency in cortical bone, i.e., $\alpha = \beta\ f$ (Minonzio et al., 2011). This linear approximation, or first order Taylor expansion, is valid around a central frequency f_0 as long as the frequency deviation Δf is narrow, i.e., $\Delta f / f_0 << 1$, even if the attenuation variation for larger frequency is not linear (Szabo, 1995; Yousefian et al., 2021). Note that the real part k of the wavenumber is assumed to be frequency independent within the considered bandwidth. With this plane wave model, the modulus of the ratio of the spectra of the two echoes (from the periosteal and endosteal surfaces) is proportional to $\exp(-\beta f 2Ct.Th)$ (Zheng et al., 2009). Note that the ultrasound signal does not need to be corrected for the overlying soft tissues, as we are studying the ratio between endosteal and periosteal echoes.Both echoes are indeed equally affected by the propagation within the soft tissue layer. Thus, the ratio only depends on the propagation inside the cortical bone layer.

Following Kuc (Kuc et al., 1976), the attenuation coefficient β can be estimated from pulse-echo measurements with a parametric approach from the shift of the center frequency of the Gaussian pulse. Assuming that the central frequency variation $\Delta f = f_1 - f_2$ is small compared to the central frequency (i.e., σ_f remains unchanged), the coefficient β writes (Kuc et al., 1976; Narayana and Ophir, 1983)

$$\beta = \frac{1}{2Ct.Th} \frac{\Delta f}{\sigma_f^2}, \tag{4}$$

with the frequency in MHz and distance in mm, β is in Np.mm^{-1}.MHz^{-1}. This parametric estimation is well adapted in both transmission (Kuc et al., 1976) and reflection (Kuc, 1984) and has been successfully applied to bone on *ex vivo* specimens in both configurations (Dencks et al., 2008; Zheng et al., 2007, 2009). Finally, the cortical broadband ultrasound attenuation in dB.cm^{-1}.MHz^{-1}, is obtained as

$$\text{Ct.nBUA} = 10 \frac{20}{\ln(10)} \beta \approx 86.9\beta. \tag{5}$$

The above equations indicate that the experimental determination of nBUA or β requires the knowledge of Ct.Th. This can be obtained from the X-ray computed tomography scan of the bone, or, alternatively, from ultrasound signals as

$$\text{Ct.Th} = v_{11}\frac{\Delta t}{2}, \tag{6}$$

where $\Delta t = t_2 - t_1$, providing the longitudinal bulk wave velocity v_{11} (in mm.μs^{-1}) is known. The index "11" refers to the radial bone direction commonly denoted direction 1 in previous studies (Foiret et al., 2014; Bernard et al., 2015). In a first approach, a nominal value of v_{11} may be assumed, i.e., the velocity is supposed to be known and identical for all subjects (Karjalainen et al., 2008; Grimal and Laugier, 2019). Thus, the β coefficient may be rewritten without reference to Ct.Th, using equations (4) and (6), as

$$\beta = 2\frac{\pi}{v_{11}}\frac{\sigma_t}{\Delta t}\frac{\Delta f}{\sigma_f}. \tag{7}$$

The quality factor Q is a dimensionless parameter, classically used to describe the resonance of a resonator, usually defined by the ratio between the central frequency and the frequency bandwidth. High Q values correspond to low attenuation. It is possible to define a quality factor related bulk wave velocity v_{11} as $Q_{11}^{-1} = \dfrac{\Im(C_{11})}{\Re(C_{11})}$ (Bernard et al., 2015), where C_{11} is the complex elastic coefficient related to v_{11}. Interestingly, as we show below, Q_{11}^{-1} does not require the knowledge of the bulk wave velocity. In case of weak attenuation, i.e., $Q_{11}^{-1} \ll 1$ or $\alpha \ll k$, which is usually satisfied in cortical bone at low frequency, i.e., less than a few MHz, (Bernard et al., 2015), the quality factors writes

$$Q_{11}^{-1} \approx \frac{2\alpha}{k} \approx \frac{\beta v_{11}}{\pi}. \tag{8}$$

Which can advantageously be rewritten

$$Q_{11}^{-1} \approx \frac{1}{\pi\sigma_f^2}\frac{\Delta f}{\Delta t}, \tag{9}$$

which expression does not depend on the bulk wave velocity v_{11} but only on the parameters Δt, Δf and σ_f which can be extracted from the measured

signals. Thus, evaluating Q_{11}^{-1} to measure attenuation could be an advantage as this does not require the knowledge of the bulk wave velocity.

1.3. In vivo ultrasound measurements

This study has been approved by the ethical committee of the Committees for the protection of persons Sud-Méditerranée. A written informed consent was provided by the five healthy subjects (24-38 years old) recruited in this study. The ultrasound measurements were approximately performed in the one-third distal extremity of the left radius. Precisely, a mark with a pen was done on the upper medial part of the forearm at 7 cm from the radial styloid and the transducer was positioned on this mark. This position exactly corresponded to the center of the region of interest scanned with HR-pQCT. A 3.5 MHz-center frequency mono element transducer (Olympus V384, 25-mm diameter, - 6dB bandwidth of 2.03MHz, Webster, TX 77598, USA) was used. The transducer was connected to a wave pulse/receiver (Olympus 5077PR SQUARE, Waltham, MA 02453, USA) and an oscilloscope (PicoScope 5000 Series, Picotechnology, Cambridgeshire, United Kingdom) for data acquisition. The sampling frequency was equal to 125 MHz. Ultrasound echoes stemming from the reflection on the outer (periosteal) and inner (endosteal) cortical bone interfaces were recorded. The waveform of the received signal was displayed on the computer screen in real time. The operator ensured a correct positioning of the probe (perpendicular to interfaces) by slightly moving the probe so as to minimize the time delay between echoes. When a satisfactory position was achieved, the operator started the acquisition of 30 consecutive signals. Note that the ultrasound signal does not need to be corrected for the overlying soft tissues, as we are studying the ratio between endosteal and periosteal echoes.

In order to illustrate the validity of the linear frequency dependence of the attenuation coefficient, a typical example of *in vivo* pulse echo measurement is shown in Figure 1. The two separated echoes can be observed on Figure 1(a), while the two associated spectra $S_1(f)$ and $S_2(f)$ are shown in Figure 1(b). Those spectra were obtained by the temporal Fourier transforms of segments $s_1(t)$ and $s_2(t)$, indicated with thick lines, corresponding to 1.2 μs from each side of the envelop maxima (Karjalainen et al., 2008). Finally, on Figure 1(c), one can observe that the variation of the spectrum ratio $\ln(|S_2(f)/S_1(f)|)$ is in agreement with the slope $\Delta f/\sigma_f^2$ of the linear approximation (Kuc et al., 1976). Note that the spectral ratio method is

based on the slope evaluation, while the peak frequency method is based on Kuc's formula.

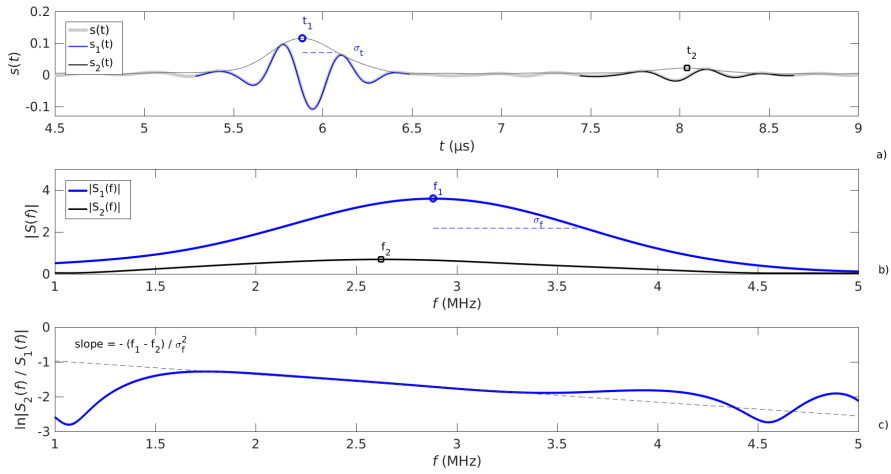

Figure 1: An example of received echoes (for subject number 3) and illustration of the linear frequency dependence of the attenuation coefficient : (a) complete temporal ultrasound signal and retained segments $s_1(t)$ and $s_2(t)$; (b) frequency spectrum of the two echoes and (c) spectrum ratio $ln(|S_2(f)/S_1(f)|)$ compared with the slope $\Delta f/\sigma_f^2$ obtained with Kuc's formula . The parameters $t_{1,2}$, $f_{1,2}$ and σ_t obtained with OMP in this study are indicated on the figures.

Processing of the signal with OMP yields the parameters (σ_{f_1}, f_1, t_1) and (σ_{f_2}, f_2, t_2) of the echoes which were used to calculate Ct.nBUA (eq. 5) using the cortical thickness value obtained from HR-pQCT (see section 1.4) (eq. 4) and Q_{11}^{-1} (eq. 9). The extraction of the parameters (σ_{t_1}, f_1, t_1) and (σ_{t_2}, f_2, t_2) is illustrated on Figure 1 using the same signal as for figure 1. It can be observed in Figure 2(b) that the retained parameters (best model number m) are associated with the two maxima, for all m, of the scalar product $< s(t)|\mathbf{d}(t; \sigma_{t_m}, f_m, t_m))| >$ between the dictionary and the signal. The maximum of this scalar product can be interpreted as the maximum quality of the signal fit, as the dictionary vectors $\mathbf{d}$ are normalized. Accordingly, for each subject, we retained the 10 (out of 30) measurements with the highest values in order to remove the poorest measurements corresponding e.g., to a poor alignment of the probe with the bone surface. The final values of nBUA and Q_{11}^{-1}, and their errors, were obtained using the mean and the standard deviation calculated on the 10 retained measurements.

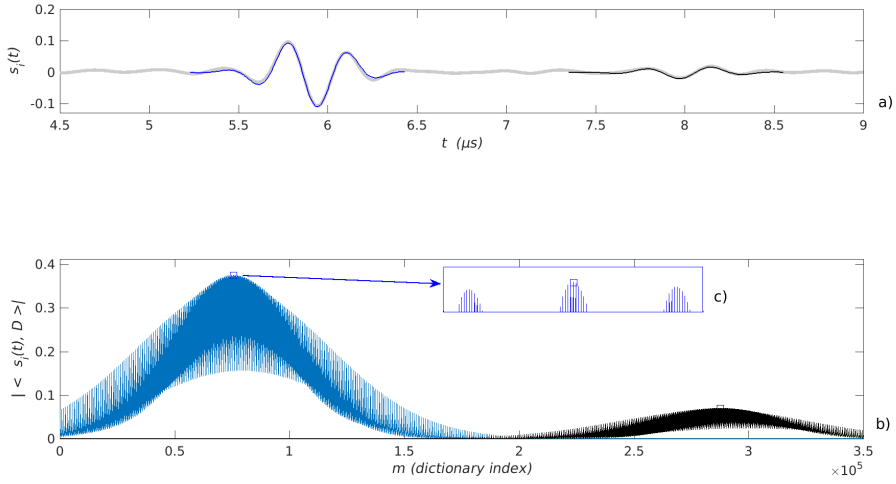

Figure 2: Principle of the evaluation of the parameters (σ_{t_m}, f_m, t_m) of the Gabor functions matching the two echoes using OMP. Original signal $y(t)$ compared with the two reconstructed echoes $s_1(t)$ (blue) and $s_2(t)$ (black) (a) associated with dictionary indices m corresponding to the two largest values of the scalar product between the signal and the dictionary (b). (c): zoom around the first maximum.

1.4. HR-pQCT

The left radius of each subject was scanned with high-resolution X-ray peripheral computed tomography (HR-pQCT, XtremeCT, Scanco Medical, Brüttisellen, Switzerland) using the standard manufacturer *in vivo* acquisition parameters (60 kVp, 1000 mA, 100 ms integration time, voxel size 82 μm). The measurements were approximately performed at the one-third distal radius site. To ensure that HR-pQCT imaging is site-matched with ultrasound measurement, we used an initial large view image allowing to center the scanning windows at 7 cm from the radial styloid corresponding to the ultrasound measurement point. The acquired volume corresponded to 9.02 mm along the bone axis (110 cross-sectional slices). The central slice is illustrated in Figure 3 for each subject. The region of interest (ROI), site-matched with the ultrasound measurement site, is highlighted. Methods used to process the CT data have been previously described in detail (Laib et al., 1998; Boutroy et al., 2005; MacNeil and Boyd, 2007; Ostertag et al., 2016). Briefly, cortical limits were determined using a threshold-based algorithm. The threshold used to discriminate cortical bone was set to one

third of the apparent cortical bone density value (Dcort). Cortical thickness was calculated for each slice as the mean distance between the periosteal and endosteal contours. Finally, the mean and standard deviation of all slice cortical thickness was retained for each subject. Volumetric bone mineral density of the cortical bone in the ROI (Ct.vBMD) was obtained directly from Dcort. The mean and standard deviation of all slice Dcort was retained for each subject.

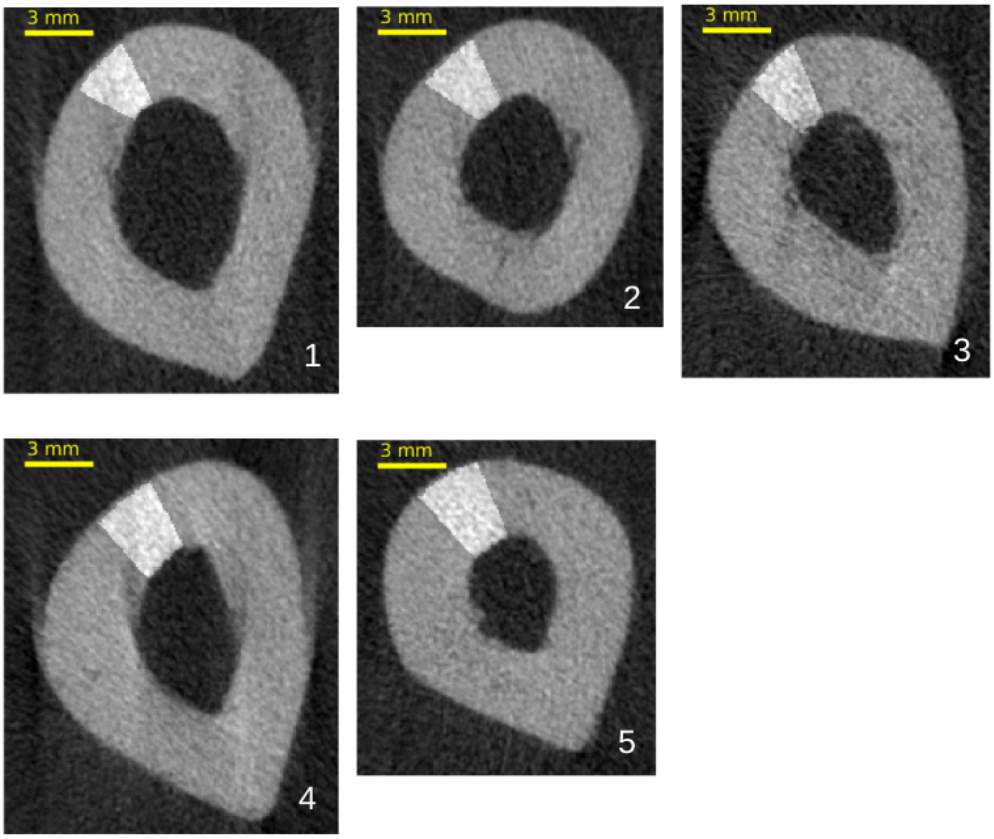

Figure 3: A representative cross-sectional HR-pQCT slice of the radius for each subject. The region of interest corresponding the ultrasound measurement site is highlighted

1.5. Data analysis

The relationships between ultrasound parameters and reference parameters obtained with HR-pQCT were assessed using linear correlations. We

report Pearson's correlation coefficient and linear regression equations.

Results

The mean and standard deviation, calculated over the ten retained measurements, of the estimated parameters Δt, Δf, σ_f for each subject are reported in Table 1. The next last column corresponds to Q_{11}^{-1} obtained combining previous parameters using equation (9). Finally, values of Ct.Th, Δf and σ_f were used to compute Ct.nBUA according to equations (4) and (5) (last column of Table 1). HR-pQCT parameters Ct.Th and Ct.vBMD are reported in Table 2.

High correlations were observed between Q_{11}^{-1} and Ct.vBMD, obtained by HR-pQCT ($R^2 = 0.93$, $p < 0.01$, RMSE= 0.76%, Fig. 4) and between Ct.nBUA and Ct.vBMD ($R^2 = 0.92, p < 0.01$, RMSE $= 0.56$ dB.MHz^{-1}.cm^{-1}, Fig. 5). The linear regression equation was Ct.nBUA $= -34.1 \times$ Ct.vBMD $+$ 45.6, where Ct.nBUA is expressed in dB.MHz^{-1}.cm^{-1} and Ct.vBMD in g.cm^{-3}. Likewise, the second linear regression equation was $Q_{11}^{-1} = -49.2 \times$ Ct.vBMD $+ 64.9$, where Q_{11}^{-1} is expressed in % and Ct.vBMD in g.cm^{-3}. The corresponding longitudinal bulk wave velocities v_{11}, ranging from 3.2 to 3.9 $mm.\mu s^{-1}$, are given in Table 3 for comparison with other studies.

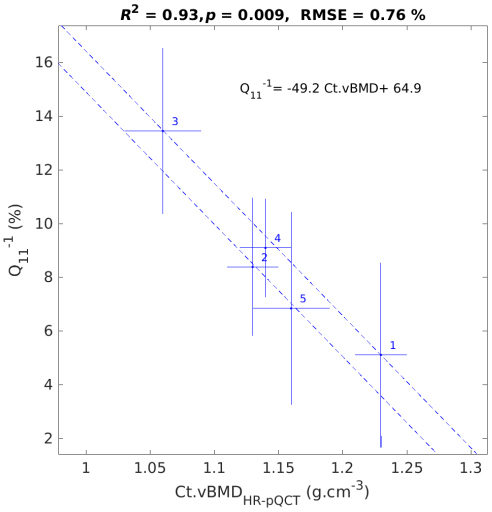

Figure 4: Correlation between quality factor Q_{11}^{-1} obtained by pulse echo and Ct.vBMD obtained by HR-pQCT.

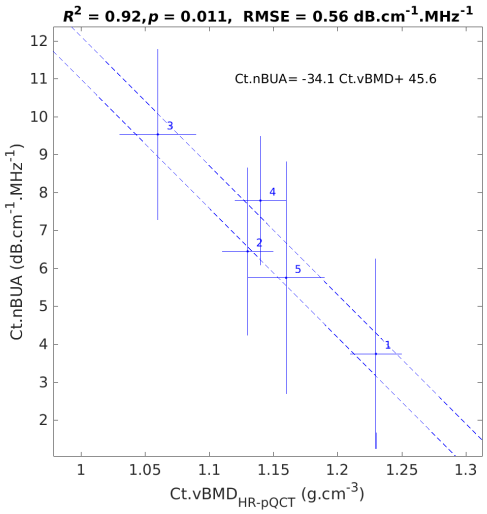

Figure 5: Correlation between Ct.nBUA and Ct.vBMD.

Discussion

This work considered pulse-echo measurements to measure the attenuation of signals from ultrasonic waves propagating in cortical bone at the radius *in vivo*. The two echoes stemming from normal-incidence reflections on the periosteal and endosteal bone surfaces were modeled as the sum of two elementary waveforms (Gabor functions), and the parameters of these waveforms (time delay, central frequency and frequency bandwidth) were recovered using sparse signal processing (OMP). Attenuation was assessed in two ways: (1) as Ct.nBUA with a parametric method using OMP parameters combined with Ct.Th from HR-pQCT ; and (2) as a quality factor Q_{11}^{-1} calculated from OMP parameters only.

The values of Ct.nBUA (6.7±2.2 dB.MHz.$^{-1}$.cm^{-1}) are in the range of the attenuation values reported in the literature on bovine and human femur (Table 4). To which extent Ct.nBUA and Q_{11}^{-1} reflect the true (intrinsic) ultrasonic attenuation in cortical bone remains to be investigated. Such quantity can only be evaluated *ex vivo* using dedicated experimental conditions in order to minimize the effect of diffraction and other losses unrelated to attenuation within the tissue.

We found that Ct.nBUA was strongly correlated to volumetric bone mineral density (Ct.vBMD) measured from X-ray attenuation ($R^2 = 0.92$, Fig.5).

This finding is in line with the *ex vivo* results of Sasso et al. (Sasso et al., 2008) who reported a correlation between Ct.nBUA and Ct.vBMD in bovine bone measured *ex vivo* ($R^2 = 0.57$, $p < 10^{-5}$, RMSE=1.6). These authors also reported the linear fit equation between Ct.nBUA and Ct.vBMD (Ct.nBUA $= -25.2 \times$ Ct.vBMD $+ 40.6$) which can be compared to our result (Ct.nBUA $= -34.1 \times$ Ct.vBMD $+ 45.6$). The differences between these equations may in part be due to the Ct.vBMD range which was different in the two studies: [1.15-1.65] g.cm^{-3} in (Sasso et al., 2008) compared [1.05-1.22] g.cm^{-3} in the present study.

Quality factor Q_{11}^{-1} (Table 1) values associated to the propagation of a longitudinal wave can be compared to shear mode quality factor Q_{44}^{-1} measured from the first resonance peak (falling in the range [100–300 kHz]) of a cuboid bone specimen (Bernard et al., 2015). In the latter study, the average Q_{44}^{-1} was 3.5% to be compared to a mean value of 8.6% in the present study. These values compare well although the comparison should be made with caution because (i) Q_{44}^{-1} was obtained at a much lower frequency (one order of magnitude); (ii) the polarization is different and a larger attenuation is expected for shear waves; (iii) the collection of samples used in (Bernard et al., 2015) includes low density (high porosity) samples which may not be representative of the bone of healthy volunteers in the present study.

Ct.nBUA was calculated from measured ultrasound parameters and a value of Ct.Th obtained from the HR-pQCT image of each subject. If only ultrasound data is available, the quality factor Q_{11}^{-1} can be calculated as it does not depend on the bulk wave velocity (Eq. 9). Our results suggest that Q_{11}^{-1} could be of clinical interest as it is correlated with Ct.vBMD ($R^2 = 0.92$, Fig.4). Furthermore, Fan et al. (2021) have shown that the shear wave quality factor is correlated to porosity (R^2=0.53), and it is reasonable to infer that Q_{11}^{-1} measured in this study is also related to porosity.

Signal parameters were estimated in the ultrasound signal with OMP, which has several advantages. The segmentation of the two echoes in the time domain was performed automatically in a robust manner, which can be an advantage in case of overlapping of echoes (which can occur for thin cortices). Also, because the Gabor function offers a reliable parametrization of the echoes, the calculation of Fourier domain parameters is done avoiding a Fourier transform of the signal which can be polluted by the choice of the time window for time segmentation.

The parametric method used to estimate attenuation relies on the measurement of Δf. In equation (7), β is written in terms of temporal and

frequency shifts divided by their associated standard deviations, leading to normalized shifts or Z-scores. Using equations (8), ${Q_{11}}^{-1}$ can also be written in term of these ratios as $\frac{\Delta f}{\sigma_f} = \frac{1}{2}{Q_{11}}^{-1}\frac{\Delta t}{\sigma_t}$. As the ratio $\Delta t/\sigma_t$ is of the order of 1 and Q_{11}^{-1} is small compared to 1, one can expect the ratio $\Delta f/\sigma_f$ to be also small compared to 1 in accordance with the weak attenuation hypothesis. Thus, special attention should be paid to the evaluation of Δf. Indeed, it can be observed in Table 1 that the largest relative uncertainties, up to 70%, are obtained for the frequency Δf parameter, while the uncertainties on the temporal Δt parameter are about a few percents. This observation should be taken into account in order to propose a robust clinical measurement.

The calculation of Ct.nBUA requires the knowledge of cortical thickness Ct.Th, which was obtained from HR-pQCT in the present proof-of-concept study. Our method to measure attenuation could however be implemented together with other ultrasound sequences and signal processing providing speed of sound and cortical thickness as described in Renaud et al. (2018) or Nguyen Minh et al. (2020).

This study has a number of limitations. (1) Only 5 healthy subjects were considered. The range of cortical bone properties (thickness, material properties) may not be representative of the general population or subjects with bone pathologies. (2) The endosteal interface of cortical bone of young healthy subjects is known to be quasi-plane and regular, whereas it is likely to be irregular and discontinuous for elderly subjects or patients with bone diseases as a result of age- or disease-related bone deterioration and trabecularization (Zebaze et al., 2010). Such irregular interface may give rise to a wave pattern more complex than the specular echo observed in the young subjects in the present study. Also, as the attenuation is expected to increase with porosity, the signal from the endosteal interface in osteoporostic or old patients should be weaker compared to the signals processed in this study. The applicability of our method to assess aged or diseased bone remains to be assessed. (3) Because the probe was handheld, some pulse echo acquisitions had to be discarded. We used a quality criterion provided by OMP processing based on the value of the scalar product between the recorded signal and the dictionary. This criterion is believed to be robust as it relies on the expected shape of the echo waveform. Nevertheless, reproducibility of the method should be assessed in future studies on a larger number of subjects. Moreover, all measurements have been carried out at the same central frequency of 3.5 MHz. This frequency may need to be adapted for smaller or

larger thicknesses in order to remain with an endosteal echo clearly separated and not too much attenuated. As attenuation in cortical bone may have a nonlinear dependence on frequency(Yousefian et al., 2021), attenuation values obtained at different frequencies may not be directly compared with the values obtained in the present study.

The results of this study suggest that ultrasonic quantities (Ct.nBUA and Q_{11}^{-1}) related to attenuation in cortical bone can be measured *in vivo* at the radius, which provide an information on bone quality as they were found to be highly correlated to Ct.vBMD values. Indeed, Ct.vBMD is an established biomarker of bone health related to bone porosity and mineralization (Engelke, 2017). If these results are confirmed in studies with a larger number and diversity of subjects, measurement of attenuation may be considered useful for assessing bone health. This can be combined with the measurement of cortical thickness, porosity and bulk wave velocities in multimodal cortical bone QUS evaluation methods. Future studies should investigate to which extent Ct.nBUA and Q_{11}^{-1} measured with the method of this study reflect the true (intrinsic) ultrasonic attenuation in cortical bone. Advanced signal processing techniques such as neural network (Mohanty et al., 2019), machine learning (Minonzio et al., 2020) or deep learning (Li et al., 2021) will be investigated in order to improve the robustness of the approach.

Acknowledgements

This work was supported by the GEP scholarship granted by the Guangzhou scholar and ANID ECOS200061 exchange programs. Jean-Gabriel Minonzio is supported by Grant ANID / FONDECYT / REGULAR / 1201311. The authors would like to thank Sylvie Fernandez and Christine Chappard (University Denis Diderot, CNRS, Osteo-Articular Bioengineering and Bioimaging (B2OA) 10, Avenue de Verdun, 75010 Paris, France) for the HR-pQCT measurements.

APPENDIX: Orthogonal Matching Pursuit

Dictionary

To implement the sparse signal processing method, the first issue is to discretize the Gabor functions into an over-complete dictionary $\mathbf{D}$, where the columns of $\mathbf{D}$ are built resorting to the Gabor functions basis

$$\mathbf{d}(t, \mathbf{\Theta}) = \zeta_{\mathbf{\Theta}} \exp[-s(t-\tau)^2] \exp[j2\pi f(t-\tau)] \quad (.1)$$
$$\mathbf{\Theta} = [s, \tau, f] \quad (.2)$$

where $\zeta_{\mathbf{\Theta}}$ is a normalization parameter that ensures $\|\mathbf{d}(\mathbf{\Theta}, t)\|_2 = 1$ (l_2-norm). To build a suitable elementary atom of $\mathbf{D}$, the columns use a discretization of the different parameters that characterize each Gabor function. The possible values of the set of parameters $\mathbf{\Theta}$ are sampled on M discrete points. For this purpose, we define an *a priori* range for s, τ, and f, these ranges being subdivided into L, S and K regular intervals, respectively. Furthermore, each Gabor function is sampled at N_t discrete time points $\mathbf{t} = [t_1, t_2, \cdots, t_{N_t}]$. The dimension of the over-complete dictionary is $M = L \times S \times K$, with $M \gg N_t$. The dictionary can be represented as

$$\mathbf{D} = \begin{bmatrix} d(t_1, \Theta_1) & d(t_1, \Theta_2) & \cdots & d(t_1, \Theta_M) \\ d(t_2, \Theta_1) & d(t_2, \Theta_2) & \cdots & d(t_2, \Theta_M) \\ \vdots & \vdots & \ddots & \vdots \\ d(t_{N_t}, \Theta_1) & d(t_{N_t}, \Theta_2) & \cdots & d(t_{N_t}, \Theta_M) \end{bmatrix} \quad (.3)$$

where

$$\Theta_m = [s_l, \tau_s, f_k], \quad l \in [1, L], s \in [1, S], k \in [1, K], m \in [1, M].$$

The ranges of variations of s, τ and k are defined as follows. The range of frequency f can be obtained from the bandwidth of the received signal, as discussed in (Mor et al., 2010). Similarly, the range for the bandwidth factor s can be deduced from the bandwidth of the emitted signal. The time delays τ of the different echoes are searched around the peaks of the envelope of the received signal. Overall, the selection of the parameter intervals is quite flexible due to the robustness and efficiency of the OMP method. Using the dictionary, the signal model (1) can be represented as

$$\mathbf{y} = \mathbf{D}\mathbf{x} + \mathbf{n} \quad (.4)$$

where $\mathbf{y}$ and $\mathbf{n}$ are the sampling of $y(t)$ and $n(t)$ at discrete time points respectively, $\mathbf{x}$ is the amplitude vector corresponding to each column in $\mathbf{D}$.

This dictionary can be interpreted as an extension of the classical Fourier transform. In the case of the temporal Fourier transform, Θ is reduced to

the frequency f and a element of the dictionary matrix writes as $d(t, \Theta) = d(t, f) = exp(-j2\pi ft)$ and previous equation, i.e., the signal reconstruction, corresponds to the inverse Fourier transform. In case of the Gabor basis, the reconstruction is sparse, i.e., only a finite number of function are necessary for reconstruction, contrary to the Fourier basis for which the reconstruction is continuous.

We evaluated the numerical cost of the OMP algorithm. For a dictionary size varying from 1000×50000 ($N_t = 1000; L = 20, K = 10, S = 250$) to 1000×80000 ($N_t = 1000; L = 20, K = 10, S = 400$), the computation time ranges approximately between 0.2 and 0.7 s on a standard personal computer (Intel(R) Xeon(R) CPU E5-2620 v2 at 2.10GHz, 32Gbytes memory, Dell, USA).

Orthogonal Matching Pursuit with complex dictionary

The application considered in this paper is the reconstruction the echoes from the periosteal and endosteal surfaces of the cortical bone. Accordingly, we restrain our analysis to the two first echoes, thus we set $P = 2$ in (1). As a consequence, we expect only 2 non-zero components of $\mathbf{x}$, which is much smaller than its dimension (M). The determination of the two main echoes requires only two iterations using sparsity constrained OMP. Since the columns of the dictionary defined in (3) are complex-valued, the corresponding steps of the OMP have to be adapted. Each iteration step consists in searching the best matching column with the residual from the previous iteration. In the case of a complex dictionary, the matching between a particular complex column and the given signal r is (Lu and Michaels, 2008)

$$< \mathbf{r}, \mathbf{d}^H >= \mathbf{d}^H \mathbf{r} = Ce^{j\phi} \tag{.5}$$

where $\mathbf{r}$ is the residual signal from last iteration, H denotes the complex conjugate transpose operator, C indicates the matching level and ϕ the phase of the residual.

The best correlated column from the dictionary $\mathbf{D}$ corresponds to the largest value of C. The corresponding position index in vector $\mathbf{x}$ is denoted

$$i_{max} = \max_i \{|\mathbf{D}(:, i)^H \mathbf{r}|\}, \tag{.6}$$

and the phase is given by

$$\phi = \text{angle}\{\mathbf{D}(:, i_{max})^H \mathbf{r}\}. \tag{.7}$$

It should be noticed that the residual cannot be iterated directly, since it is defined as the linear combination of two real Gaussian pulses instead of complex-values Gabor functions as introduced in (.1). After computation of (.6) and (.7), The real Gaussian pulses $\mathbf{D}_r(i_{max})$ are obtained using the relationship

$$\mathbf{D}_r(:, i_{max}) = \Re\{\mathbf{D}(:, i_{max})e^{-j\phi}\}. \tag{.8}$$

The OMP processing is illustrated in Algorithm 1.

Algorithm 1 Orthogonal Matching Pursuit algorithm

Input: $\mathbf{y} \in \mathbb{R}^N$, $\mathbf{D} \in \mathbb{C}^{N \times M}$, target sparsity=2

Output: sparse solution $\mathbf{x} \in \mathbb{R}^M$

Set $I = ()$, $\mathbf{r} = \mathbf{y}$, $\mathbf{D}_r = \mathbf{D}(:, I)$

for target sparsity **do**

  $i_{max} = \max_i |\mathbf{D}(:, i)^H \mathbf{r}|$

  $\mathbf{I} = (\mathbf{I}, \mathbf{i_{max}})$

  $\phi = \text{angle}\{\mathbf{D}(:, i_{max})^H \mathbf{r}\}$

  $\mathbf{D}_r(:, i_{max}) = \Re\{\mathbf{D}(:, i_{max})e^{-j\phi}\}$

  $\mathbf{x}(I) = \mathbf{D}_r(:, I)^\dagger \mathbf{y}$ † denotes pseudo inverse

  $\mathbf{r} = \mathbf{y} - \mathbf{D}_r(:, I)\mathbf{x}(I)$

end for

References

Bala Y, Zebaze R, Ghasem-Zadeh A, Atkinson EJ, Iuliano S, Peterson JM, Amin S, Bjørnerem Å, Melton LJ, Johansson H, Kanis JA, Khosla S, Seeman E. Cortical Porosity Identifies Women With Osteopenia at Increased Risk for Forearm Fractures. Journal of Bone and Mineral Research, 2014;29:1356–1362.

Bernard S, Schneider J, Varga P, Laugier P, Raum K, Grimal Q. Elasticity–density and viscoelasticity–density relationships at the tibia mid-diaphysis assessed from resonant ultrasound spectroscopy measurements. Biomechanics and Modeling in Mechanobiology, 2015;15:97–109.

Boutroy S, Bouxsein ML, Munoz F, Delmas PD. In Vivo Assessment of Trabecular Bone Microarchitecture by High-Resolution Peripheral Quantitative Computed Tomography. The Journal of Clinical Endocrinology & Metabolism, 2005;90:6508–6515.

Briot K, Paternotte S, Kolta S, Eastell R, Felsenberg D, Reid DM, Glüer CC, Roux C. FRAX®: Prediction of Major Osteoporotic Fractures in Women from the General Population: The OPUS Study. PLoS ONE, 2013;8:e83436.

Choksi P, Jepsen KJ, Clines GA. The challenges of diagnosing osteoporosis and the limitations of currently available tools. Clinical diabetes and endocrinology, 2018;4:12.

Demirli R, Saniie J. Model-based estimation of ultrasonic echoes. Part II: Nondestructive evaluation applications. IEEE Transactions on Ultrasonics, Ferroelectrics and Frequency Control, 2001;48:803–811.

Dencks S, Barkmann R, Padilla F, Laugier P, Schmitz G, Gluer CC. Model-based estimation of quantitative ultrasound variables at the proximal femur. IEEE Transactions on Ultrasonics, Ferroelectrics and Frequency Control, 2008;55:1304–1315.

Engelke K. Quantitative Computed Tomography—Current Status and New Developments. Journal of Clinical Densitometry, 2017.

Fan F, Cai X, Follet H, Peyrin F, Laugier P, Niu H, Grimal Q. Cortical bone viscoelastic damping assessed with resonant ultrasound spectroscopy

reflects porosity and mineral content. Journal of the Mechanical Behavior of Biomedical Materials, 2021;117:104388.

Foiret J, Minonzio JG, Chappard C, Talmant M, Laugier P. Combined estimation of thickness and velocities using ultrasound guided waves: A pioneering study on in vitro cortical bone samples. IEEE Transactions on Ultrasonics, Ferroelectrics, and Frequency Control, 2014;61:1478–1488.

Grimal Q, Laugier P. Quantitative ultrasound assessment of cortical bone properties beyond bone mineral density. IRBM, 2019;40:16–24.

Han S, Rho J, Medige J, Ziv1 I. Ultrasound velocity and broadband attenuation over a wide range of bone mineral density. Osteoporosis International, 1996;6:291–296.

Holzer G, von Skrbensky G, Holzer LA, Pichl W. Hip Fractures and the Contribution of Cortical Versus Trabecular Bone to Femoral Neck Strength. Journal of Bone and Mineral Research, 2009;24:468–474.

Iori G, Du J, Hackenbeck J, Kilappa V, Raum K. Estimation of Cortical Bone Microstructure from Ultrasound Backscatter. IEEE Transactions on Ultrasonics, Ferroelectrics, and Frequency Control, 2020.

Karjalainen J, Riekkinen O, Toyras J, Kroger H, Jurvelin J. Ultrasonic assessment of cortical bone thickness in vitro and in vivo. IEEE Transactions on Ultrasonics, Ferroelectrics and Frequency Control, 2008;55:2191–2197.

Kral R, Osima M, Borgen TT, Vestgaard R, Richardsen E, Åshild Bjørnerem. Increased cortical porosity and reduced cortical thickness of the proximal femur are associated with nonvertebral fracture independent of fracture risk assessment tool and garvan estimates in postmenopausal women. PlosOne, 2017;12:e0185363.

Kuc R. Estimating acoustic attenuation from reflected ultrasound signals: Comparison of spectral-shift and spectral-difference approaches. IEEE Transactions on Ultrasonics, Ferroelectrics and Frequency Control, 1984;32:1–6.

Kuc R, Schwartz M, Micsky LV. Parametric Estimation of the Acoustic Attenuation Coefficient Slope for Soft Tissue. In: 1976 Ultrasonics Symposium. IEEE, 1976. pp. 44–47.

Laib A, Häuselmann H, Rüegsegger P. In vivo high resolution 3D-QCT of the human forearm. Technol Health Care, 1998;6:329–337.

Lakes R, Yoon HS, Katz JL. Ultrasonic wave propagation and attenuation in wet bone. Journal of Biomedical Engineering, 1986;8:143–148.

Langton CM, Njeh CF. The measurement of broadband ultrasonic attenuation in cancellous bone-a review of the science and technology. IEEE Transactions on Ultrasonics, Ferroelectrics, and Frequency Control, 2008;55:1546–1554.

Lees S, Klopholz DZ. Sonic velocity and attenuation in wet compact cow femur for the frequency range 5 to 100 MHz. Ultrasound in Medicine & Biology, 1992;18:303–308.

Li Y, Xu K, Li Y, Xu F, Ta D, Wang W. Deep learning analysis of ultrasonic guided waves for cortical bone characterization. IEEE Transactions on Ultrasonics, Ferroelectrics, and Frequency Control, 2021;68:935–951.

Lu Y, Michaels JE. Numerical implementation of matching pursuit for the analysis of complex ultrasonic signals. IEEE Transactions on Ultrasonics, Ferroelectrics and Frequency Control, 2008;55:173–182.

MacNeil JA, Boyd SK. Accuracy of high-resolution peripheral quantitative computed tomography for measurement of bone quality. Med Eng Phys, 2007;29:1096–1105.

Mamou J, Oelze ML. Quantitative Ultrasound in Soft Tissues. Springer, 2013.

Minonzio JG, Bochud N, Vallet Q, Ramiandrisoa D, Etcheto A, Briot K, Kolta S, Roux C, Laugier P. Ultrasound-Based Estimates of Cortical Bone Thickness and Porosity Are Associated With Nontraumatic Fractures in Postmenopausal Women: A Pilot Study. Journal of Bone and Mineral Research, 2019;34:1585–1596.

Minonzio JG, Cataldo B, Olivares R, Ramiandrisoa D, Soto R, Crawford B, De Albuquerque VHC, Munoz R. Automatic classifying of patients with non-traumatic fractures based on ultrasonic guided wave spectrum image using a dynamic support vector machine. IEEE Access, 2020;8:194752–194764.

Minonzio JG, Foiret J, Talmant M, Laugier P. Impact of attenuation on guided mode wavenumber measurement in axial transmission on bone mimicking plates. The Journal of the Acoustical Society of America, 2011;130:3574–3582.

Mohanty K, Yousefian O, Karbalaeisadegh Y, Ulrich M, Grimal Q, Muller M. Artificial neural network to estimate micro-architectural properties of cortical bone using ultrasonic attenuation: A 2-d numerical study. Computers in Biology and Medicine, 2019;114:103457.

Moilanen P. Ultrasonic guided waves in bone. IEEE Transactions on Ultrasonics, Ferroelectrics and Frequency Control, 2008;55:1277–1286.

Mor E, Azoulay A, Aladjem M. A matching pursuit method for approximating overlapping ultrasonic echoes. IEEE Transactions on Ultrasonics, Ferroelectrics and Frequency Control, 2010;57:1996–2004.

Narayana PA, Ophir J. On the validity of the linear approximation in the parametric measurement of attenuation in tissues. Ultrasound in Medicine and Biology, 1983;9:357–361.

Nguyen Minh H, Du J, Raum K. Estimation of Thickness and Speed of Sound in Cortical Bone Using Multifocus Pulse-Echo Ultrasound. IEEE Transactions on Ultrasonics, Ferroelectrics, and Frequency Control, 2020;67:568–579.

Nishiyama KK, Macdonald HM, Buie HR, Hanley DA, Boyd SK. Postmenopausal Women With Osteopenia Have Higher Cortical Porosity and Thinner Cortices at the Distal Radius and Tibia Than Women With Normal aBMD: An In VivoHR-pQCT Study. Journal of Bone and Mineral Research, 2010:882–890.

Ostertag A, Peyrin F, Gouttenoire PJ, Laredo J, DeVernejoul M, Cohen-Solal M, Chappard C. Multiscale and multimodality computed tomography for cortical bone analysis. Physics in medicine and biology, 2016;61:8553–8576.

Paranhos Neto F, Vieira Neto L, Madeira M, Moraes A, Mendonça L, Lima I, Chagas C, Lira D, Spitz J, Guimarães J, Duarte M, Farias M. Vitamin d deficiency is associated with cortical bone loss and fractures in the elderly. European journal of endocrinology, 2019;181:509—-517.

Renaud G, Clouzet P, Cassereau D, Talmant M. Measuring anisotropy of elastic wave velocity with ultrasound imaging and an autofocus method - application to cortical bone. Physics in medicine and biology, 2020.

Renaud G, Kruizinga P, Cassereau D, Laugier P. In vivo ultrasound imaging of the bone cortex. Physics in Medicine & Biology, 2018;63:125010.

Sai H, Iguchi G, Tobimatsu T, Takahashi K, Otani T, Horii K, Mano I, Nagai I, Iio H, Fujita T, Yoh K, Baba H. Novel ultrasonic bone densitometry based on two longitudinal waves: significant correlation with pQCT measurement values and age-related changes in trabecular bone density, cortical thickness, and elastic modulus of trabecular bone in a normal Japanese population. Osteoporosis International, 2010;21:1781–1790.

Sasso M, Haïat G, Yamato Y, Naili S, Matsukawa M. Dependence of ultrasonic attenuation on bone mass and microstructure in bovine cortical bone. Journal of Biomechanics, 2008;41:347–355.

Siris E. Absolute Versus Relative Fracture Risk. Journal of Bone and Mineral Research, 2004;20:705–705.

Szabo TL. Causal theories and data for acoustic attenuation obeying a frequency power law. The Journal of the Acoustical Society of America, 1995;97:14–24.

Talmant M, Renaud G, Grimal Q. Measurement of ultrasonic anisotropic attenuation of P-wave in millimeter-sized human cortical bone samples. In: 8th International Symposium on Ultrasonic Characterization of Bone, 2019.

Tropp JA, Gilbert AC. Signal recovery from random measurements via orthogonal matching pursuit. IEEE Transactions on Information Theory, 2007;53:4655–4666.

Yousefian O, Karbalaeisadegh Y, Muller M. Frequency-dependent analysis of ultrasound apparent absorption coefficient in multiple scattering porous media: application to cortical bone. Physics in Medicine and Biology, 2021;66.

Yousefian O, White RD, Karbalaeisadegh Y, Banks HT, Muller M. The effect of pore size and density on ultrasonic attenuation in porous structures

with mono-disperse random pore distribution: A two-dimensional in-silico study. The Journal of the Acoustical Society of America, 2018.

Zebaze RM, Ghasem-Zadeh A, Bohte A, Iuliano-Burns S, Mirams M, Price RI, Mackie EJ, Seeman E. Intracortical remodelling and porosity in the distal radius and post-mortem femurs of women: a cross-sectional study. The Lancet, 2010;375:1729–1736.

Zheng R, Le LH, Sacchi MD, Lou E. Broadband ultrasound attenuation measurement of long bone using peak frequency of the echoes. IEEE Transactions on Ultrasonics, Ferroelectrics and Frequency Control, 2009;56:396–399.

Zheng R, Le LH, Sacchi MD, Ta D, Lou E. Spectral ratio method to estimate broadband ultrasound attenuation of cortical bones in vitrousing multiple reflections. Physics in Medicine & Biology, 2007;52:5855–5869.

Tables

Table 1: Ultrasound measurements: Δt is the arrival time difference between the two echoes, Δf is the shift of central frequency, σ_f is related to the frequency bandwidth. The quality factor Q_{11}^{-1} is calculated from these three quantities and Ct.nBUA is calculated using the ultrasound measurements and Ct.Th measured with Ht-pQCT.

Subject No.	Δt (μs)	Δf (MHz)	σ_f (MHz)	Q_{11}^{-1} (%)	Ct.nBUA (dB.MHz^{-1}.cm^{-1})
1	1.67±0.02	0.21±0.15	0.94±0.03	5.1±3.4	3.7±2.5
2	1.75±0.04	0.34±0.13	1.05±0.19	8.4±2.6	6.5±2.2
3	1.70±0.02	0.46±0.07	0.81±0.02	13.5±3.1	9.5±2.3
4	2.14±0.08	0.51±0.11	0.93±0.06	9.1±1.8	7.8±1.7
5	2.32±0.04	0.37±0.16	0.89±0.06	6.8±3.6	5.8±3.1
mean ± std	1.92±0.30	0.38±0.12	0.92±0.09	8.6±3.1	6.7±2.2

Table 2: Cortical thickness (Ct.Th) and volumetric bone mineral density (Ct.vBMD) obtained from HR-pQCT images.

	HR-pQCT	
Subject No.	Ct.Th (mm)	Ct.vBMD ($g.cm^{-3}$)
1	3.11±0.08	1.23±0.02
2	3.13±0.02	1.13±0.02
3	3.28±0.06	1.06±0.03
4	3.43±0.02	1.14±0.02
5	3.79±0.03	1.16±0.03
mean ± std	3.35±0.28	1.14±0.06

Table 3: Longitudinal bulk wave velocities calculated as $v_{11} = 2\text{Ct.Th}/\Delta t$ using values given in Tables 1 and 2

Subject No.	v_{11} $(mm.\mu s^{-1})$
1	3.72±0.14
2	3.58±0.10
3	3.86±0.12
4	3.21±0.14
5	3.27±0.08
mean ± std	3.53±0.28

Table 4: Normalized broadband ultrasonic attenuation (nBUA) values published in the scientific literature and in this study. Mean values are given, and standard deviation when available.

* In Talmant et al. (2019), the reported attenuation normal to the direction of osteons is, at 4 MHz, 3.9 dB.cm^{-1} per percentage of porosity ; the value given in the table is calculated for a very moderate porosity of 5% characteristic of the bone of a healthy young adult.

Reference	Species and skeletal sites	Number of samples	Frequency range or center frequency (MHz)	nBUA (dB MHz^{-1}cm^{-1})
Lakes et al. (1986)(Lakes et al., 1986)	bovine femur (*ex vivo*)	1	1-7	∼3
Lees and Klopholtz (1992)(Lees and Klopholz, 1992)	bovine femur (*ex vivo*)	4	0-30	∼4
Han et al. (1996)(Han et al., 1996)	bovine femur (*ex vivo*)	5	0.3-0.7	5 - 12
Zheng et al.(2007)(Zheng et al., 2007)	bovine femur (*ex vivo*)	8	2.25	4.91±0.65
Sasso et al.(2008)(Sasso et al., 2008)	bovine femur (*ex vivo*)	40	3.5-4.5	4.2±2.4
Talmant et al. (2019) *	human femur (*ex vivo*)	35	2-8	4.9
This paper	one-third distal radius (*in vivo*)	5	3.5	6.7± 2.2